# A Study on Interfacial Reactions between Electroless Ni-P Under Bump Metallization and 95.5Sn-4.0Ag-0.5Cu Alloy

YOUNG-DOO JEON,[1,3] SABINE NIELAND,[2] ANDREAS OSTMANN,[2] HERBERT REICHL,[2] and KYUNG-WOOK PAIK[1]

1.—Department of Materials Science and Engineering, Korea Advanced Institute of Science and Technology, Taejon 305-701, Korea. 2.—Department of Chip Interconnection Technology, Fraunhofer IZM, Germany. 3.—E-mail: doo@kaist.ac.kr

Even though electroless Ni-P and Sn-Ag-Cu solders are widely used materials in flip-chip bumping technologies, interfacial reactions of the ternary Cu-Ni-Sn system are not well understood. The growth of intermetallic compounds (IMCs) at the under bump metallization (UBM)/solder interface can affect solder-joint reliability, so analysis of IMC phases and understanding their growth kinetics are important. In this study, interfacial reactions between electroless Ni-P UBM and the 95.5Sn-4.0Ag-0.5Cu alloy were investigated, focusing on identification of IMC phases and IMC growth kinetics at various reflowing and aging temperatures and times. The stable ternary IMC initially formed at the interface after reflowing was the $(Cu,Ni)_6Sn_5$ phase. However, during aging, the $(Cu,Ni)_6Sn_5$ phase slowly changed into the quaternary IMC composed of Cu, Ni, Sn, and a small amount of Au. The Au atoms in the quaternary IMC originated from immersion Au plated on electroless Ni-P UBM. During further reflowing or aging, the $(Ni,Cu)_3Sn_4$ IMC started forming because of the limited Cu content in the solder. Morphology, composition, and crystal structure of each IMC were identified using transmission electron microscopy (TEM) and scanning electron microscopy (SEM). Small amounts of Cu in the solder affect the types of IMC phases and the amount of the IMC. The activation energies of $(Cu,Ni)_6Sn_5$ and $(Ni,Cu)_3Sn_4$ IMCs were used to estimate the growth kinetics of IMCs. The growth of IMCs formed in aging was very slow and temperature-dependent compared to IMCs formed in reflow because of the higher activation energies of IMCs in aging. Comparing activation energies of each IMC, growth mechanism of IMCs at electroless Ni-P/SnAgCu solder interface will be discussed.

**Key words:** Electroless Ni, SnAgCu, UBM, Pb-free solder

## INTRODUCTION

Solder-bumping technology using electroless Ni-P under bump metallization (UBM) and screen-printed solder is one of the commonly used flip-chip technologies because of its cost effectiveness. Recently, the screen-printed solder-bumping technique was applied to chips with less than 200-μm input/output (I/O) pitch. In addition, electroless Ni-P UBM is known as a good barrier material for Pb-free solders because of its low reactivity with Sn. As demands for Pb-free solders are increasing, many Pb-free solder pastes are being developed. Among these Pb-free solder alloys, four candidates, Sn-3.5Ag, Sn-3.5Ag-0.7Cu (Sn-4.0Ag-0.5Cu), Sn-0.7Cu, and Sn-3.5Ag-4.8Bi, are expected to be adopted in the industry.

In this study, Sn-4.0Ag-0.5Cu solder paste was chosen, and interfacial reactions between electroless Ni-P UBM and the Sn-Ag-Cu solder bump were investigated. There are numbers of reports about the interfacial reactions between Ni-P and Sn-Ag-Cu alloy. Jang et al. observed a $Ni_4Cu_7Sn_6$ ternary IMC at the interface, and all IMCs were well attached on the UBM.[1] Kang et al. observed only the $(Ni,Cu)_3Sn_4$ IMC at the interface between electroless Ni-P and Sn-Ag-Cu.[2] Zeng et al. reported that $(Cu,Ni)_6Sn_5$ and $(Ni,Cu)_3Sn_4$ were formed above and below 0.6 at.% Cu in the solder, respectively.[3] Lee et al. reported that the quater-

(Received November 25, 2002; accepted January 20, 2003)

nary IMC might be made of the Cu-Ni-Sn IMC and $AuSn_4$ IMCs, and its activation energy was 196 kJ/mol.[4] Zirbe et al. observed $(Cu,Ni)_6Sn_5$ composed of $Cu_{27}Ni_{26}Sn_{47}$.[5] These references showed many different results in terms of IMC phases, and compositions of IMCs because ternary reactions among Ni, Cu, and Sn at the interface are very complicated. In addition, growth mechanisms of IMCs during reflow and aging are not clearly understood. Therefore, in this study, various reflow and aging conditions were performed to investigate types of IMCs and the growth mechanism. To identify IMC phases, transmission electron microscopy (TEM) was used, and crystal structures and compositions of IMCs were analyzed.

## EXPERIMENTAL PROCEDURE

The 6 μm of electroless Ni with 11–13at.%P and 0.08 μm of immersion Au were plated on Al I/O pads of test chips. Then, screen printing of Sn-4.0Ag-0.5Cu solder followed. After reflow at 250°C for 0.5 min, solder balls were fabricated, as shown in Fig. 1. After solder bumps were initially fabricated, further reflowing and aging tests were performed to investigate interfacial reactions between the liquid solder and electroless Ni and between the solid solder and electroless Ni, respectively. After flux activation at 150°C for 1 min, reflows at 260°C, 280°C, 300°C, 320°C, and 350°C for 0.5 min, 1 min, 2 min, 4 min, and 8 min were performed. On the other hand, aging tests were performed at 85°C, 125°C, 150°C, 175°C, and 200°C for 125 h, 300 h, 500 h, 1,000 h, and 2,000 h after the initial solder reflow.

Backscattered-electron image and energy dispersive x-ray spectroscopy (EDS) in SEM were used to observe interface and analyze composition (20 KeV). To identify crystal structures, electron-diffraction patterns were obtained using the selected-area diffraction pattern technique in TEM.

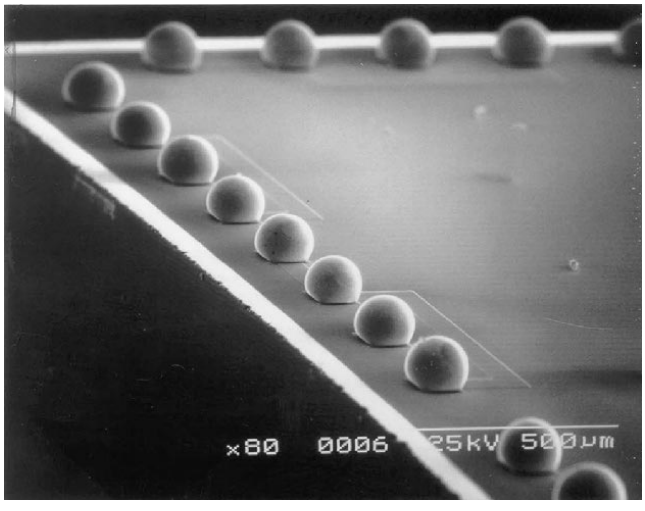


Fig. 1. The stencil-printed Sn-4.0Ag-0.5Cu solder bumps on electroless Ni-P UBMs.

## RESULTS AND DISCUSSION

### Interfacial Reactions between Electroless Ni and Liquid Sn-Ag-Cu Solder during Solder Reflowing

*Intermetallic Compounds at the Interface*

Figure 2 shows cross-sectioned solder bumps at various solder-reflow temperatures and times. It was observed that IMCs formed at the interface changed as reflow temperatures and times increased. Figure 3 shows magnified images of typical interfaces at 260°C and 320°C, respectively. Below 300°C, only one IMC was observed, as shown in Fig. 3a, and it was well attached at the UBM. The EDS results showed that this IMC was composed of 21–24at.%Ni, 27–30at.%Cu, and 48–50at.%Sn. However, two different IMCs were found at reflow temperatures higher than 300°C. In Fig. 3b, these two IMCs (IMC I and II) are clearly distinguished. The upper IMC (which looked bulky and faceted) had the same composition as the IMC in Fig. 3a (IMC I). The first formed IMC contains nearly 30at.%Cu, and its composition is very similar to $(Cu,Ni)_6Sn_5$ even though its faceted morphology differs from the scalloplike $Cu_6Sn_5$ phase. On the other hand, the IMC that looked like needle (IMC II) was composed of 31–36at.%Ni, 4–7at.%Cu, and 58–63at.%Sn. Therefore, the composition of the second forming IMC is very similar as that of $(Ni,Cu)_3Sn_4$. The morphology of each IMC was confirmed by preferential solder etching. The etching solution of 35 g/L orthonitrophenol and 50 g/L NaOH was used. Figure 4 shows the morphology of each IMC after reflow at 320°C for 1 min. The first forming IMC grew abnormally, and it had facetlike morphology. In the same figure, the second forming IMC

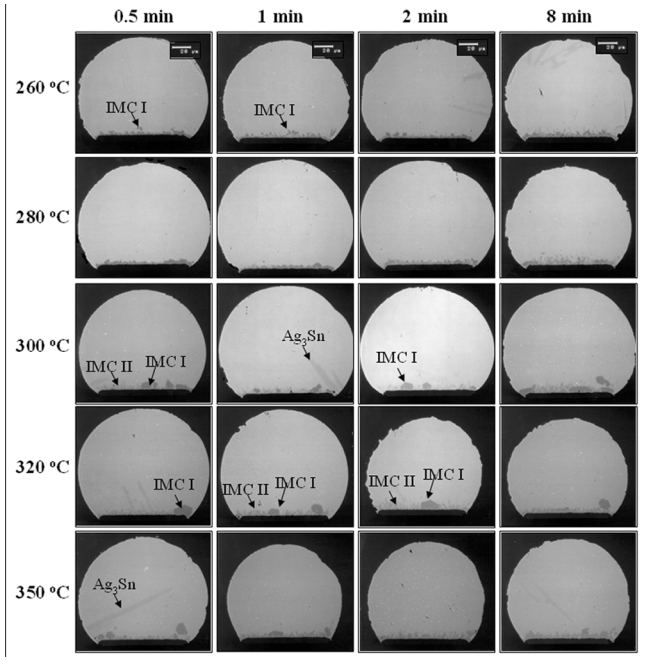


Fig. 2. The cross-sectional images of solder bumps at various reflow temperatures and times.

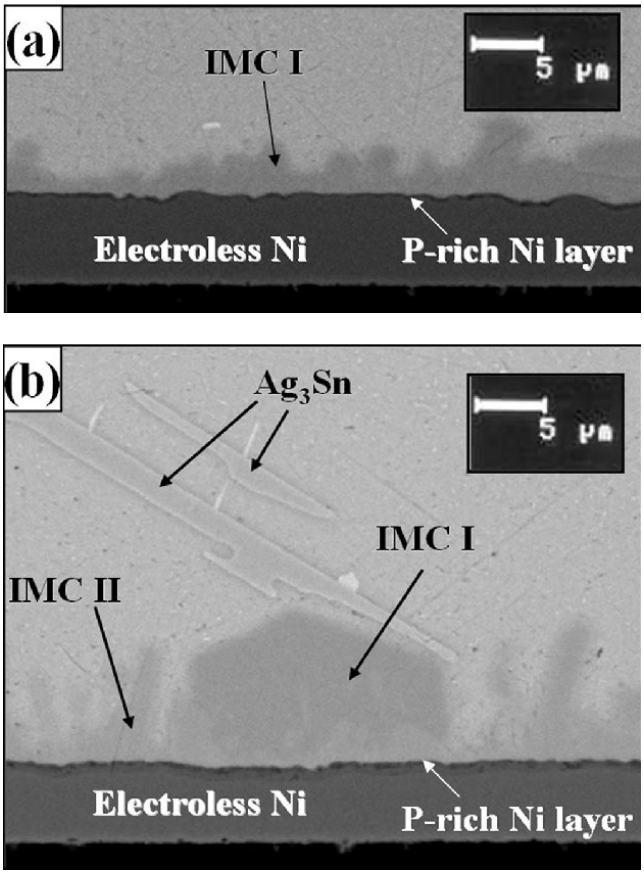


Fig. 3. The interfaces after solder reflowing at (a) 260°C for 0.5 min and (b) 320°C for 4 min.

had needlelike morphology, and it was well attached on the UBM.

The IMC phase identification cannot be clearly understood by EDS results. Therefore, electron-diffraction analysis was performed using TEM to identify each IMC phases. Figure 5a and b shows TEM images of these two IMCs after solder reflow at 320°C for 8 min. Electron-diffraction patterns of each IMCs are shown in Fig. 6. The electron-diffraction patterns in Fig. 6a and c were exactly matched to the crystal structure of $Cu_6Sn_5$ (Fig. 6b and d). Therefore, the first forming IMC must be the $(Cu,Ni)_6Sn_5$ phase, where 21–24at.%Ni atoms substitute for the Cu position in the Cu sublattice. Presumably, the faceted morphology of the $(Cu,Ni)_6Sn_5$ IMC might be caused by addition of 21–24 at.%Ni. Electron-diffraction patterns of the second forming IMC (Fig. 6e and g) were the same as the crystal structure of the $Ni_3Sn_4$ phase (Fig. 6f and h). Therefore, the phase of this IMC must be the $(Ni,Cu)_3Sn_4$ phase that consists of the $Ni_3Sn_4$-crystal structure with 4–7at.%Cu atoms in the Ni sublattice.

The IMC phase that formed first was not $(Ni,Cu)_3Sn_4$ but $(Cu,Ni)_6Sn_5$ even though the Cu content (0.5 wt.%) in the solder is extremely low compared to Ni and Sn. Therefore, the thermodynamic-IMC phase in equilibrium at the Cu-Ni-Sn interface is

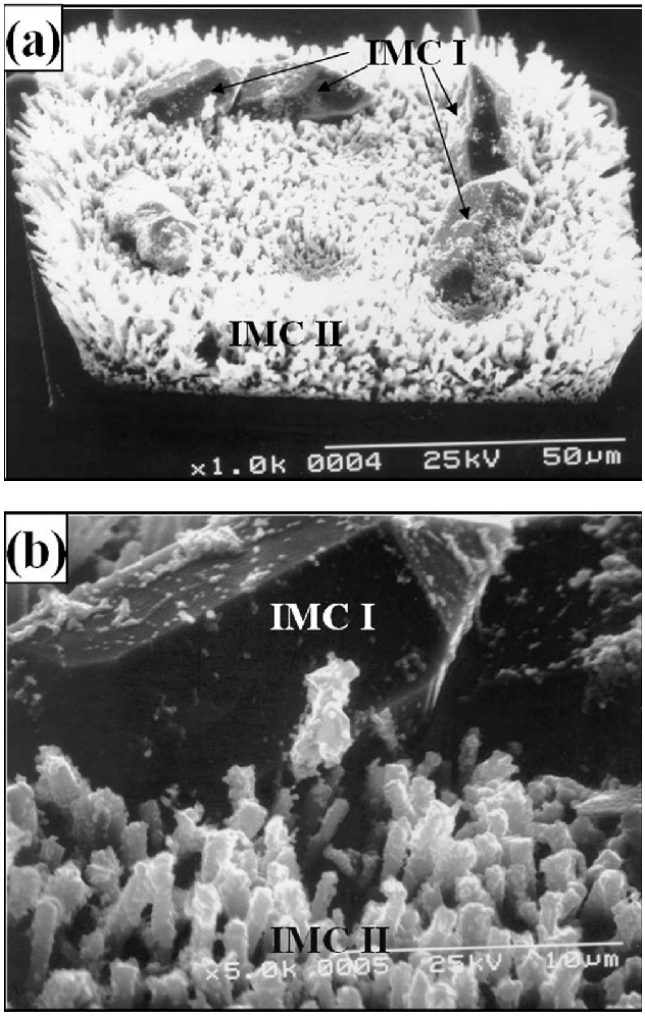


Fig. 4. The morphologies of IMCs after solder reflowing at 320°C for 1 min: (a) ×1,000 and (b) ×5,000.

$(Cu,Ni)_6Sn_5$ rather than $(Ni,Cu)_3Sn_4$. If no Cu is available for diffusing into the interface, the $(Ni,Cu)_3Sn_4$ phase starts forming during additional solder reflows. The formation of the $(Cu,Ni)_6Sn_5$ phase might be impossible because of the limited content of Cu in the solder. This result means that a small amount of Cu in the solder significantly affects the formation process of the IMC and the total amount of IMCs at the interface. If there was no Cu in the solder, the $Ni_3Sn_4$ IMC would be stable and consumption of Ni would be much higher because $Ni_3Sn_4$ needed more Ni than $(Cu,Ni)_6Sn_5$. Formation of the $(Cu,Ni)_6Sn_5$ IMC in Cu-contained solder probably reduce the consumption rate of the electroless Ni-P UBM.

Figure 7 is schematic diagram showing how the interface changes as reflow continues. In the early stage of reflow, the $(Cu,Ni)_6Sn_5$ IMC formed and was well attached on the UBM (Figs. 3a and 7a). During additional reflows, the $(Cu,Ni)_6Sn_5$ IMC stopped growing and a needlelike $(Ni,Cu)_3Sn_4$ IMC started growing underneath the $(Cu,Ni)_6Sn_5$ IMC (Fig. 7b). Finally, the $(Cu,Ni)_6Sn_5$ IMC became bigger and had facetlike morphology. Some grains of the $(Cu,Ni)_6Sn_5$

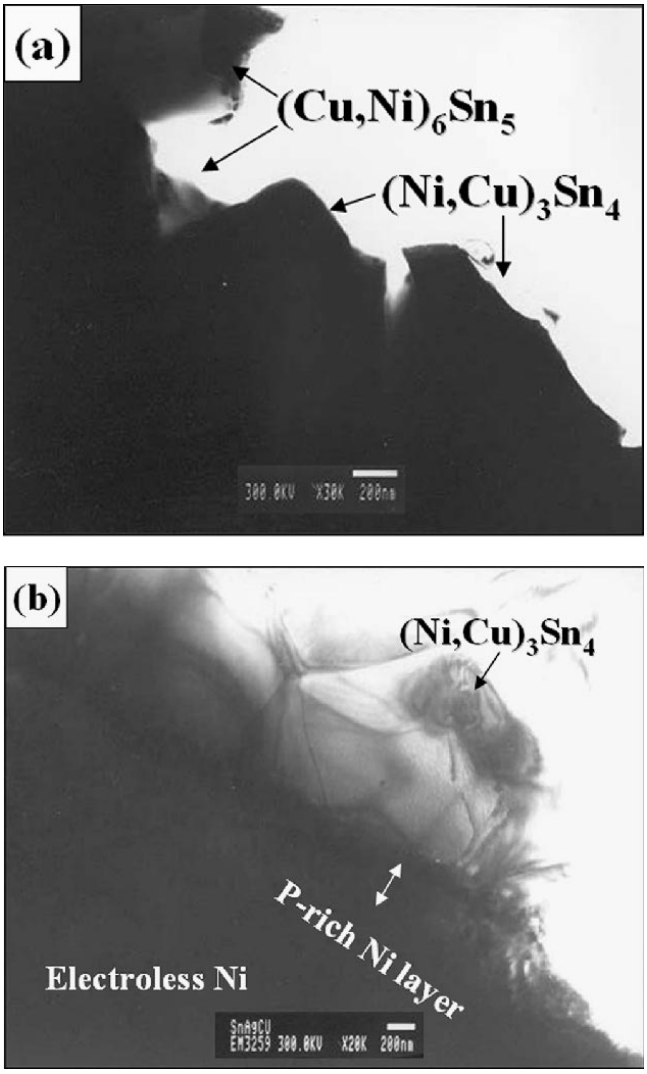


Fig. 5. The TEM images of the $(Cu,Ni)_6Sn_5$ and $(Ni,Cu)_3Sn_4$ IMCs after solder reflowing at 320°C for 8 min.

IMC were separated from the interface and started spalling into the molten solder (Fig. 7c). A number of references reported that IMCs at the interface between the electroless Ni and the Sn-Ag-Cu alloy were well attached on the UBM.[1,2,4] However, in this study, it was found that $(Cu,Ni)_6Sn_5$ IMCs formed in an excessive reflowing condition grow abnormally and spall into the solder.

*Growth Kinetics of Intermetallic Compounds*

To simplify growth kinetics of IMCs, the following assumptions were considered.

- Solubility of Ni in molten solder is independent of the reflow temperature.
- During the reflow process, growth of the IMC is considered only at the molten-solder region of the IMC. The IMC growth during heating and cooling is negligible.
- To reduce errors by the second assumption, durations for heating and cooling were set as short as possible. The power law and the Arrhenius equation were applied as follows:

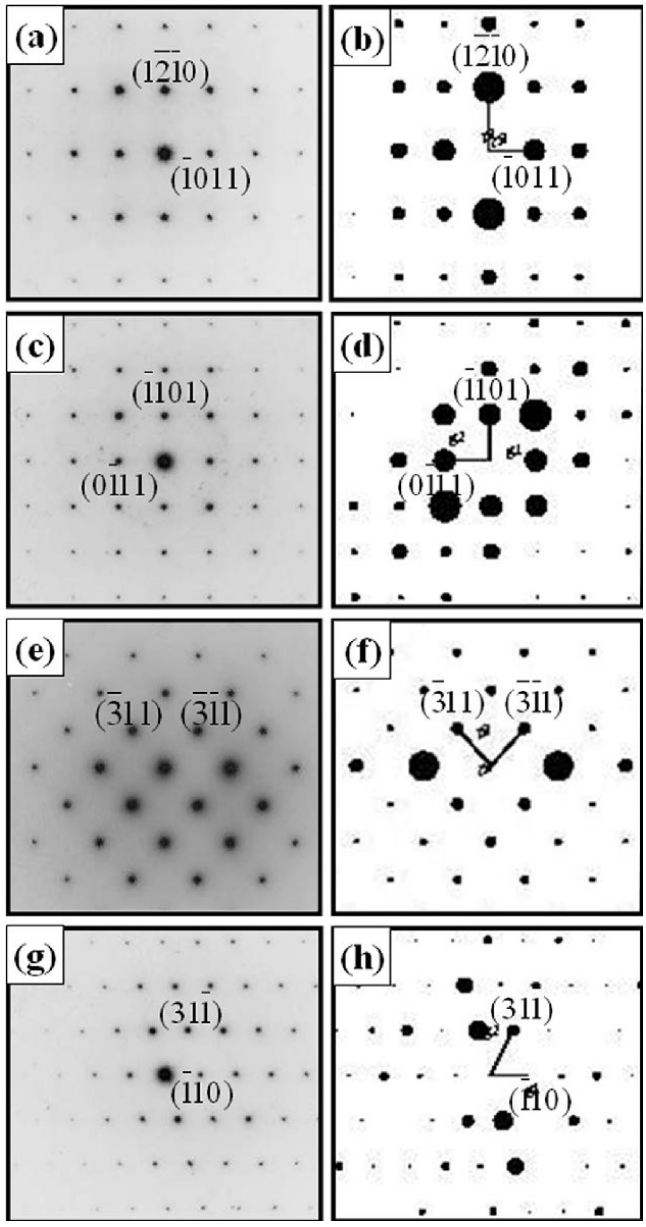


Fig. 6. The electron-diffraction patterns of the $(Cu,Ni)_6Sn_5$ and $(Ni,Cu)_3Sn_4$ IMCs: (a) $(Cu,Ni)_6Sn_5$ [2,1,−3,2], (b) simulation result of $Cu_6Sn_5$ [2,1,−3,2], (c) $(Cu,Ni)_6Sn_5$ [2,1,−3,1], (d) simulation result of $Cu_6Sn_5$ [2,1,−3,1], (e) $(Ni,Cu)_3Sn_4$ [−1,0,−3], (f) simulation result of $Ni_3Sn_4$ [−1,0,−3], (g) $(Ni,Cu)_3Sn_4$ [−1,−1,4], and (h) simulation result of $Ni_3Sn_4$ [−1,−1,4].

$$\text{Power law: } d = d_0 + t^n \quad (1)$$

$$\text{Arrhenius equation: } d = d_o + A \exp(-\Delta Q_A/RT) \quad (2)$$

$$\text{Equation for growth kinetics: } d = d_o + At^n \exp(-\Delta Q_A/RT) \quad (3)$$

Growth kinetics of IMCs can be estimated by measuring the thickness of the IMCs at various conditions. However, it is difficult to measure the exact thickness of IMCs because IMCs generally have

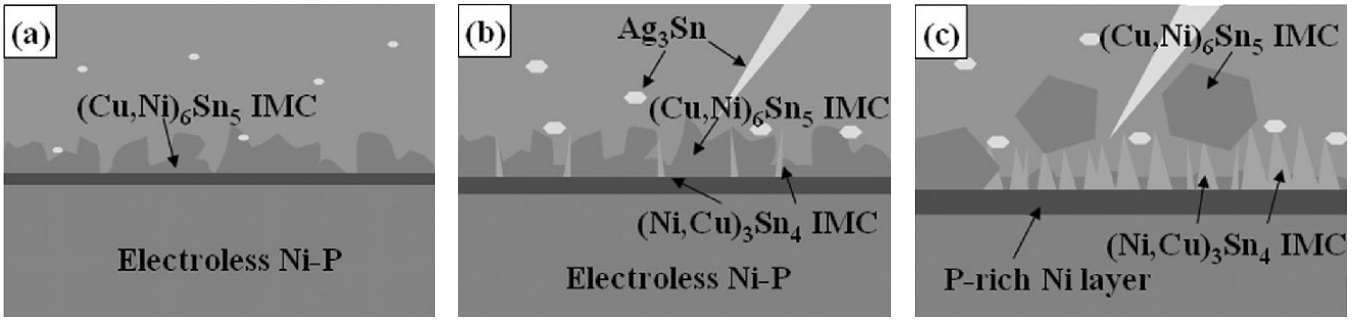


Fig. 7. The schematic diagrams of IMC growth during reflows: (a) early stage, (b) middle stage, and (c) final stage.

complicated morphology. Therefore, a measurement of UBM thickness can be useful to estimate growth of IMCs because decreasing UBM thickness by UBM consumption is proportional to IMCs thickness increase. Equation 4 shows that activation energy of IMC growth can be obtained as functions of $\Delta T_{UBM}$ and 1/T.

$$\Delta T_{IMC} = C \cdot \Delta T_{UBM},\ C < 0\text{: assumption}$$

$$\ln(\Delta T_{IMC}) = -\frac{\Delta Q_{IMC}}{R} \cdot \frac{1}{T} + \ln(A) \quad (4\text{-}1)$$

$$\ln(C \cdot \Delta T_{UBM}) = -\frac{\Delta Q_{IMC}}{R} \cdot \frac{1}{T} + \ln(A) \quad (4\text{-}2)$$

$$\ln(-C) + \ln(-\Delta T_{UBM}) = -\frac{\Delta Q_{IMC}}{R} \cdot \frac{1}{T} + \ln(A) \quad (4\text{-}3)$$

$$\ln(-\Delta T_{UBM}) = -\frac{\Delta Q_{IMC}}{R} \cdot \frac{1}{T} + \ln(A) - \ln(-C) \quad (4\text{-}4)$$

where $\Delta T_{IMC}$ is the thickness change of IMCs, $\Delta T_{UBM}$ is the thickness change of the electroless Ni UBM, $\Delta Q_{IMC}$ is the activation energy of the IMCs growth, T is temperature, R is the gas constant, and A and C are constants.

Figure 8 shows the consumption of the electroless Ni-P UBM as a function of reflow temperature and time. When each graph was fitted by the power law, the exponent, n, was approximately 0.41. This value is between 0.5, the ideal diffusion-controlled model, and 0.33, the grain-boundary diffusion-controlled model.[6] There is a clear difference in consumption rate between curves below 300°C and those above 300°C. Below 300°C, UBM consumption was rapid as reflow temperatures increased. However, the graphs above 300°C shows that UBM consumption does not decrease significantly even at 350°C reflow. Therefore, there are some IMC growth-mechanism changes at the 300°C reflow condition, and it is related to the formation of the two IMCs explained previously. In Fig. 2, a transition from the $(Cu,Ni)_6Sn_5$ IMC to the $(Ni,Cu)_3Sn_4$ IMC started at 300°C.

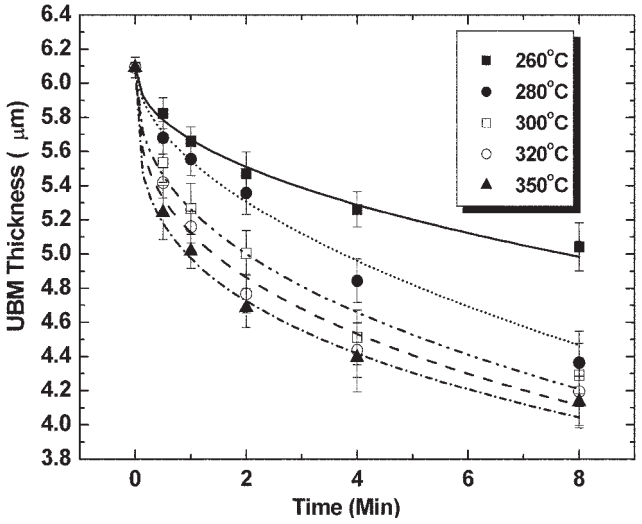


Fig. 8. The consumption of electroless Ni-P UBM at various reflow temperatures and times.

Figure 9 shows Arrhenius plots at various reflow times from 0.5–8 min. The activation energy can be obtained by measuring the slope of the curves. It was observed that the slope of curves changed abruptly at certain temperatures. In short-time reflows, such as 0.5 min, 1 min, 2 min, and 4 min, the transition temperature was about 300°C, but in 8-min reflow, the transition temperature decreased to about 280°C. As mentioned previously, the transition-temperature change from 300°C to 280°C is due to the change of IMC phases from $(Cu,Ni)_6Sn_5$ to $(Ni,Cu)_3Sn_4$. When the $(Ni,Cu)_3Sn_4$ IMC started forming, the slope of the Arrhenius curve decreased abruptly. The activation energies of the $(Cu,Ni)_6Sn_5$ and $(Ni,Cu)_3Sn_4$ IMCs were 45–61 kJ/mol and 5–24 kJ/mol, respectively. A higher activation energy of the $(Cu,Ni)_6Sn_5$ IMC means its growth is more temperature-dependent.

The high activation energy of the $(Cu,Ni)_6Sn_5$ IMC must be closely related to the diffusion of Cu atoms. Because of the very low content of Cu in the solder, diffusion of Cu is the most crucial factor in forming the $(Cu,Ni)_6Sn_5$ IMC. Diffusion of Cu atoms can be greatly increased by a slight increase of reflow temperature even at lower than 300°C reflow temperature. However, when the $(Ni,Cu)_3Sn_4$ IMC

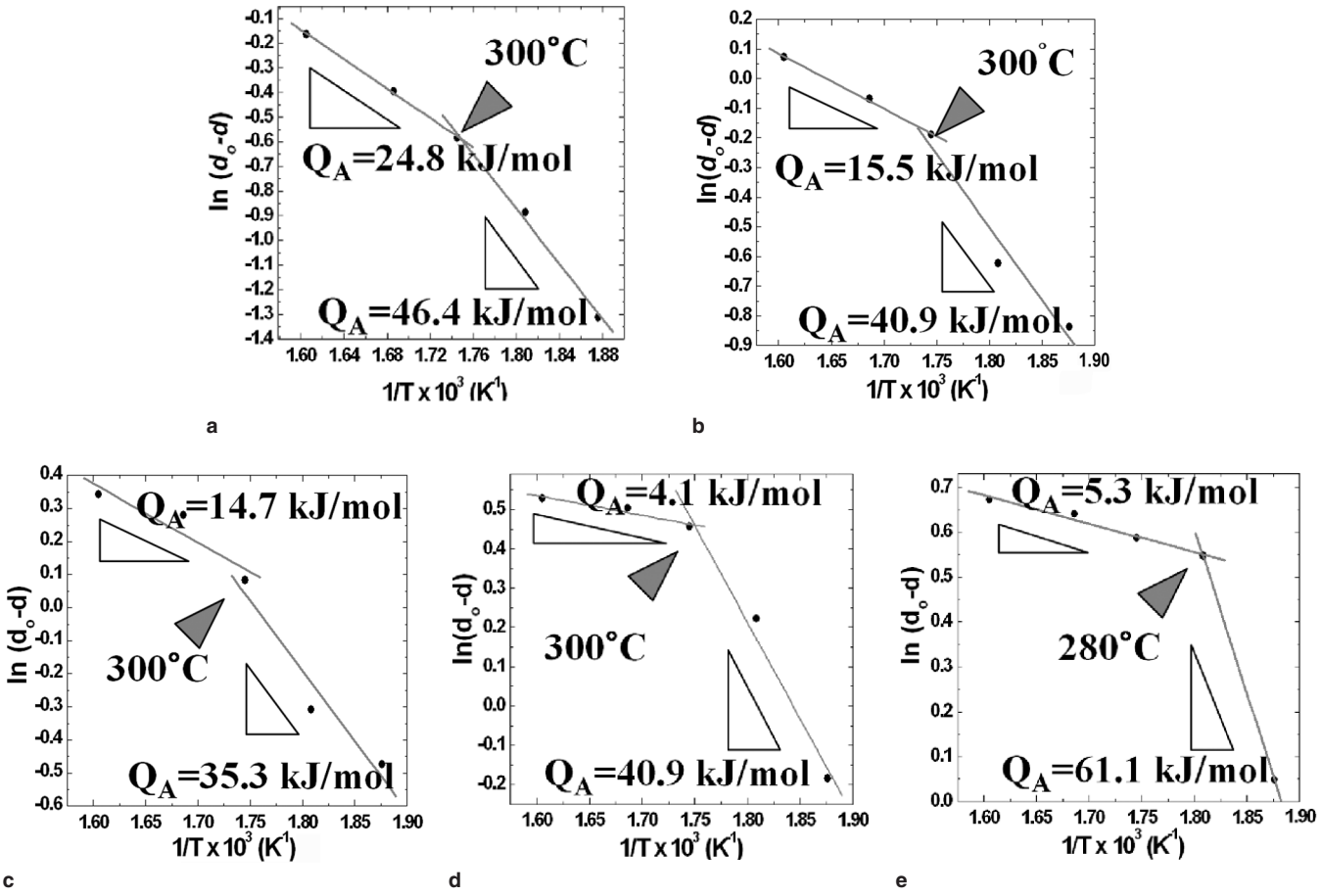


Fig. 9. The Arrhenius plots of ln (d − $d_0$) versus 1/T at various reflow times: (a) 0.5 min, (b) 1 min, (c) 2 min, (d) 4 min, and (e) 8 min.

forms at over 300°C reflow temperature, plenty of Ni and Sn atoms can easily diffuse, resulting in less susceptibility to reflow temperature.

*$Ag_3Sn$ Intermetallic Compound*

The $Ag_3Sn$ IMC was frequently observed in solder bumps. However, it was found that some of the $Ag_3Sn$ IMC grew as big as solder bump size. Figure 10 shows an abnormally grown $Ag_3Sn$ IMC after preferential solder etching. The important thing is that the $Ag_3Sn$ IMC can grow abnormally even in a very short reflow time (30 sec), which means the growth rate of the $Ag_3Sn$ IMC is extremely fast. Solder-joint reliability may be affected by large $Ag_3Sn$ IMCs; however, this is not clearly understood.

## Interfacial Reactions between Electroless Ni UBM and Solid Solder during Aging

*Intermetallic Compounds at the Interface*

Figure 11 shows cross-sectional images of solder bumps after thermal aging at various temperatures and times. In general, IMCs grow as aging temperatures and times increase. Especially, after aging at 175°C and 200°C, two kinds of IMCs were observed. In contrast to IMCs after solder reflowing, all IMCs were formed with a layered structure, and abnormal growth and spalling of IMCs were not observed. However, after aging at 200°C over 500 h, all of the electroless Ni-P UBM layer was consumed. And then, IMCs started spalling because IMCs were not wettable with the Al pad.

Figure 12 shows the solder/UBM interface after aging. Like reflowing, the first forming IMC during aging was the $(Cu,Ni)_6Sn_5$ phase (Fig. 12a). At higher temperature aging, the $(Cu,Ni)_6Sn_5$ IMC slowly changed to a brighter phase at the top of the $(Cu,Ni)_6Sn_5$ IMC (Fig. 12b). This brighter IMC was analyzed as a quaternary phase composed of 19–22at.%Ni, 25–28at.%Cu, 46–48at.%Sn, and about 5at.%Au. Because of containing 5at.%Au in the $(Cu,Ni)_6Sn_5$ IMC, the IMC became heavier and looked brighter in the backscattered-electron image. This quaternary IMC was observed only after aging. A small amount of Au originated from an immersion Au-plated layer (0.08 μm). The immersion Au layer dissolves rapidly into the molten solder because the solubility of Au in molten Sn is very high. However, in the solid-solder state, Au atoms must come out of the solder because the solubility of Au in solid Sn is nearly zero. Then, Au atoms slowly accumulate on top of the $(Cu,Ni)_6Sn_5$ IMC and change the $(Cu,Ni)_6Sn_5$ IMC into the quaternary IMC. To iden-

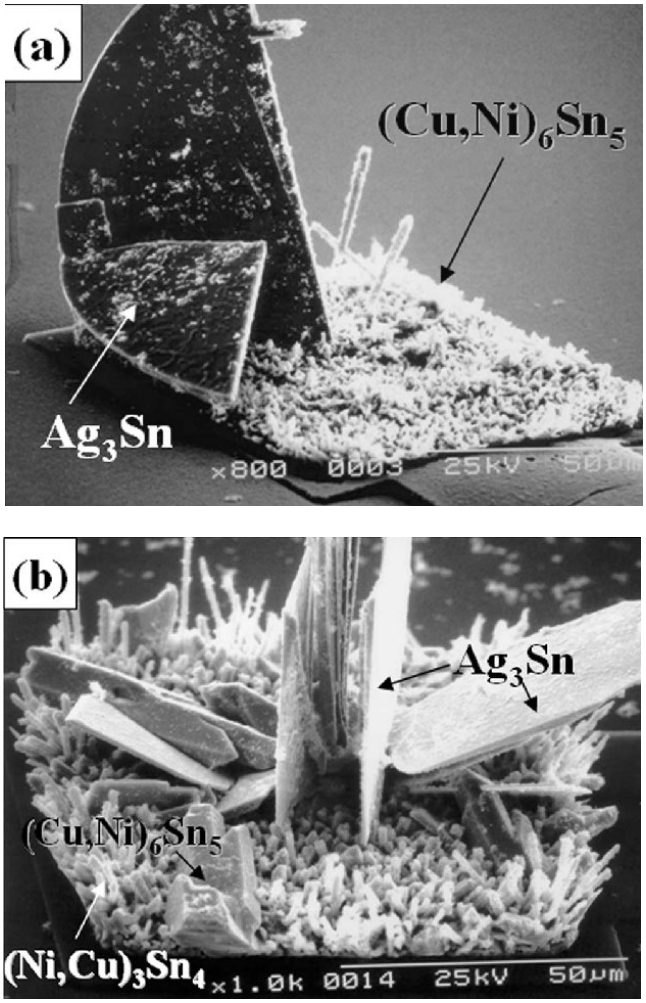


Fig. 10. The morphology of the $Ag_3Sn$ IMC: (a) after aging at 85°C for 125 h and (b) after reflow at 350°C for 2 min.

tify the crystal structure of the quaternary IMC, electron-diffraction patterns were obtained using TEM. The electron-diffraction patterns of the quaternary IMC, shown in Fig. 13a and c, were very similar to those of the $Cu_6Sn_5$ IMC (Fig. 13b and d). Strong spots were matched to the $Cu_6Sn_5$-crystal structure. However, there were two weak spots between every two strong spots. These weak spots imply that the crystal structure of the IMC may be

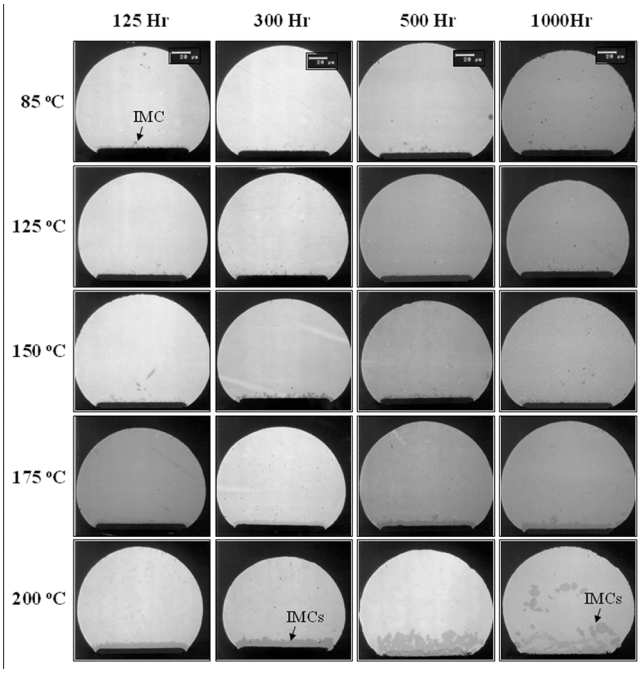


Fig. 11. The cross-sectional images of solder bumps at various aging temperatures and times.

superlattice, which is 3 times larger than the $Cu_6Sn_5$ lattice. The 5at.%Au atoms, which are orderly distributed in the $Cu_6Sn_5$ lattice, may result in weak spots in diffraction patterns.

In Fig. 12c, all of the $(Cu,Ni)_6Sn_5$ IMC changed into the quaternary IMC. A new IMC looked darker than the quaternary IMC formed at the interface between the quaternary IMC and the P-rich Ni layer during further aging. This IMC had the same composition as the $(Ni,Cu)_3Sn_4$ IMC identified at reflow treatment. The electron-diffraction pattern in Fig. 14b shows that this IMC has a $Ni_3Sn_4$-crystal structure, which was identified at reflow (Fig. 14c).

All of the quaternary IMC disappeared and changed to the $(Ni,Cu)_3Sn_4$ IMC at a higher temperature (Fig. 12d). A small amount of Au may exist in the $(Ni,Cu)_3Sn_4$ IMC, but it cannot be detectable because of the extensive volume of the $(Ni,Cu)_3Sn_4$ IMC compared with the small amount of Au. The IMC changes during thermal aging are shown schematically in Fig. 15.

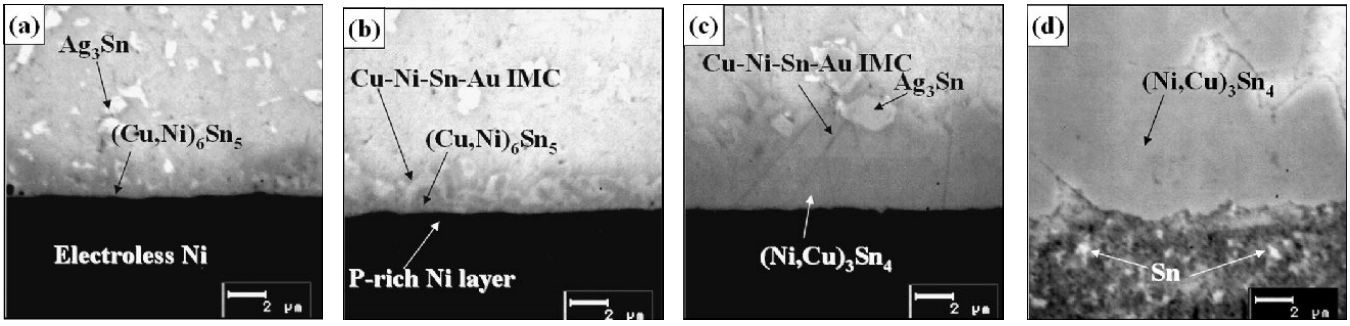


Fig. 12. The interfaces at various aging conditions: (a) 125°C, 500 h; (b) 150°C, 500 h; (c) 175°C, 500 h; and (d) 200°C, 500 h.

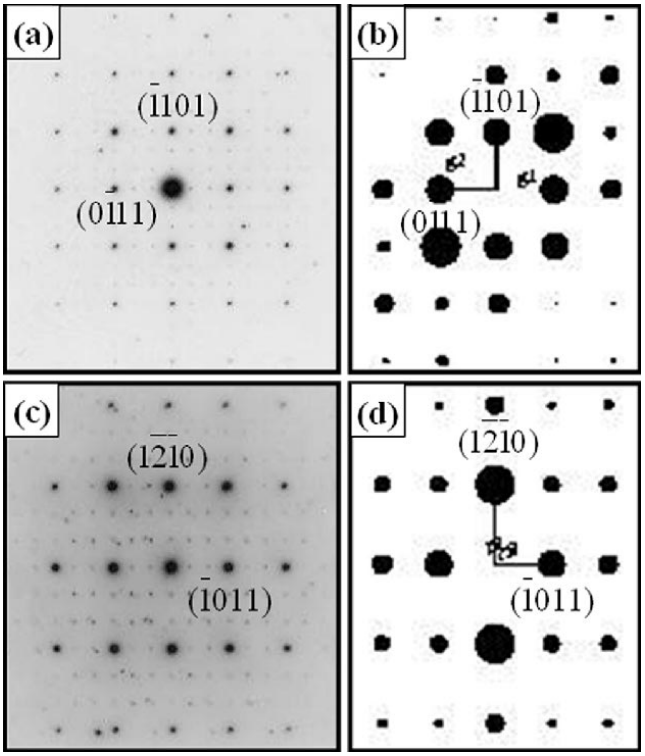


Fig. 13. The electron-diffraction patterns of the quaternary IMC: (a) quaternary IMC [2,1,−3,1], (b) simulation result of $Cu_6Sn_5$ [2,1,−3,1], (c) quaternary IMC [2,1,−3,1], and (d) simulation result of $Cu_6Sn_5$ [2,1,−3,1].

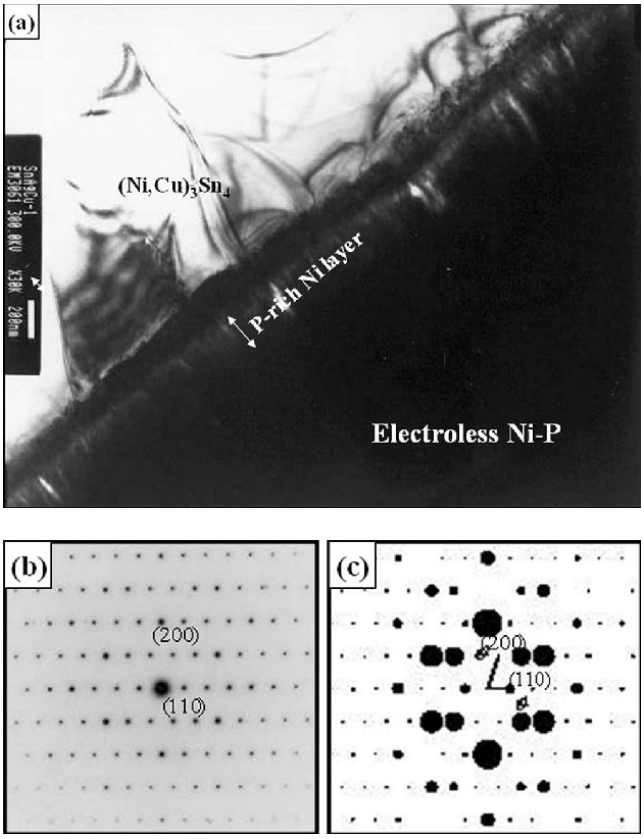


Fig. 14. The TEM analysis of the $(Ni,Cu)_3Sn_4$ IMC: (a) cross-sectioned image of the $(Ni,Cu)_3Sn_4$ IMC after aging at 200°C for 125 h, (b) the diffraction pattern of the $(Ni,Cu)_3Sn_4$ IMC [001], and (c) the simulation result of the $Ni_3Sn_4$ IMC [001].

The layered structure of IMCs can be a clue to understanding the diffusion mechanism. Figure 16 shows a schematic diagram of how Sn and Ni atoms will diffuse. To form the $(Ni,Cu)_3Sn_4$ IMC underneath the quaternary IMC layer, Sn atoms should diffuse through the quaternary IMC layer. In Fig. 12d, it was observed that Sn atoms were continuously diffusing through the IMCs, even after all the electroless Ni UBM had been consumed. Therefore, the limiting step for formation of the $(Ni,Cu)_3Sn_4$ IMC after aging must be diffusion of Sn through the quaternary IMC layer.

*Growth Kinetics of Intermetallic Compounds*

The consumption of the electroless Ni UBM layer was measured at various aging temperatures and times (Fig. 17). It was assumed that the solubility of Ni in the solid solder might be independent of aging temperature. The curves in Fig. 17 show that the consumption rate of the UBM was much faster at 175°C and 200°C than below 150°C. Figure 18 shows the Arrhenius plots at various aging times. Even though three kinds of IMCs were detected on the interface, there was no abrupt change of slope compared with ones observed in reflowing treatment. Slopes of each curve ranged between 56.2 kJ/mol and 82.0 kJ/mol, which is much higher than that observed in reflowing. Higher activation energy in aging implies that IMC formation during aging should be much more difficult than that during reflowing, and Cu can easily diffuse through the channel between irregular IMCs. However, during aging,

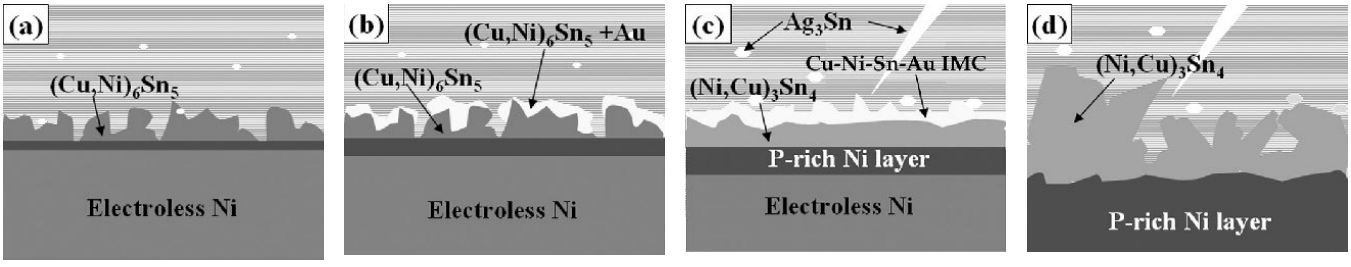


Fig. 15. The schematic diagrams of IMC changes during aging treatment: (a) early growth of the $(Cu,Ni)_6Sn_5$ IMC, (b) formation of the quaternary IMC, (c) formation of the $(Ni,Cu)_3Sn_4$ IMC, and (d) spalling of the $(Ni,Cu)_3Sn_4$ IMC.

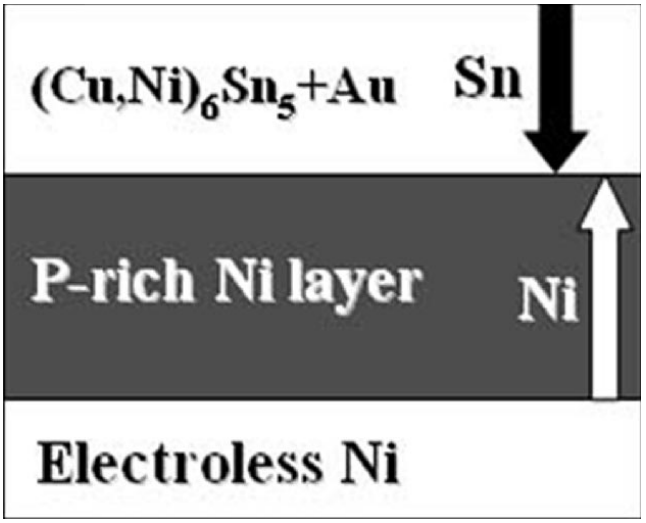


a

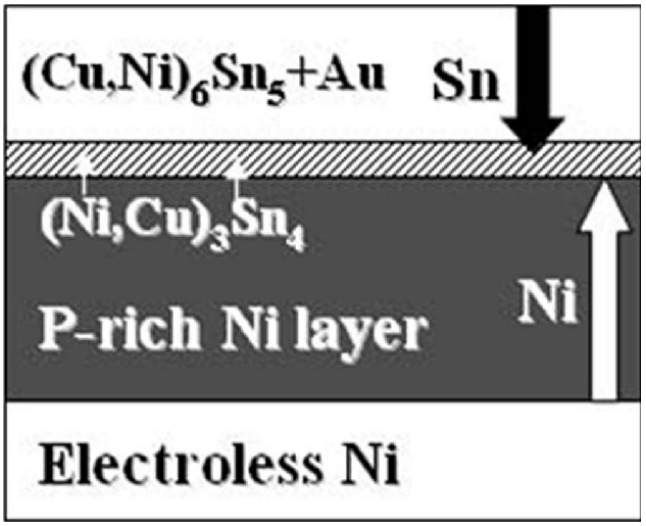


b

Fig. 16. The growth mechanism of the $(Ni,Cu)_3Sn_4$ IMC during aging treatment: (a) Sn diffusion through the quaternary IMC and (b) formation of the $(Ni,Cu)_3Sn_4$ IMC at the interface between the quaternary IMC and the P-rich Ni layer.

diffusion of Sn or Cu atoms becomes difficult because the diffusion path will be through bulky layers of IMCs or grain boundaries of IMCs.

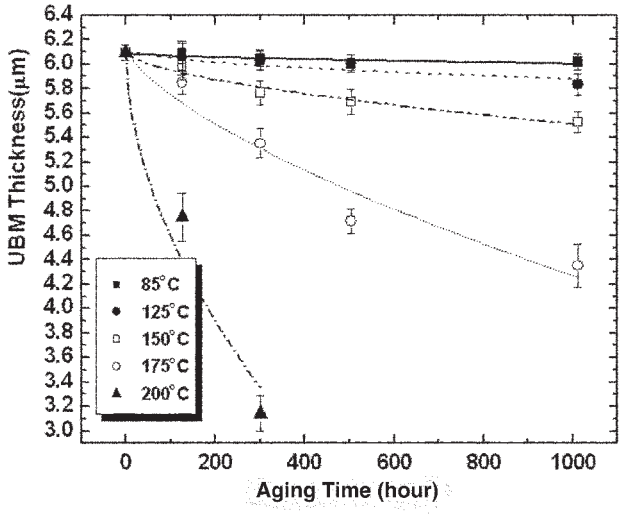


Fig. 17. Consumption of electroless Ni-P UBM at various aging temperatures and times.

## CONCLUSIONS

Interfacial reactions between electroless Ni UBM and 95.5Sn-4.0Ag-0.5Cu alloy during reflow and aging were studied. The ternary IMC that formed initially at the interface was the $(Cu,Ni)_6Sn_5$ phase in both heat treatments. The $(Cu,Ni)_6Sn_5$ phase seems to be the most equilibrium phase in the Cu-Ni-Sn ternary system. After the consumption of Cu, the $(Ni,Cu)_3Sn_4$ IMC was formed after the $(Cu,Ni)_6Sn_5$ IMC. When the $(Ni,Cu)_3Sn_4$ IMC was formed during reflowing, the $(Cu,Ni)_6Sn_5$ IMC grew abnormally and was spalled from the interface. The $(Cu,Ni)_6Sn_5$ and $(Ni,Cu)_3Sn_4$ IMCs had facetlike and needlelike morphologies, respectively. Diffusion of Cu into the interface is considered a limiting step for the formation of the $(Cu,Ni)_6Sn_5$ IMC. In addition, the formation of the $(Cu,Ni)_6Sn_5$ IMC earlier than the $(Ni,Cu)_3Sn_4$ IMC would be helpful to reduce the consumption rate of electroless Ni-P UBM. In addition, the $Ag_3Sn$ IMC can grow abnormally even in a short-time reflow, and they have big platelike morphology.

During aging, the initially formed $(Cu,Ni)_6Sn_5$ IMC slowly changed to the quaternary IMC, which is similar to the $(Cu,Ni)_6Sn_5$ IMC containing

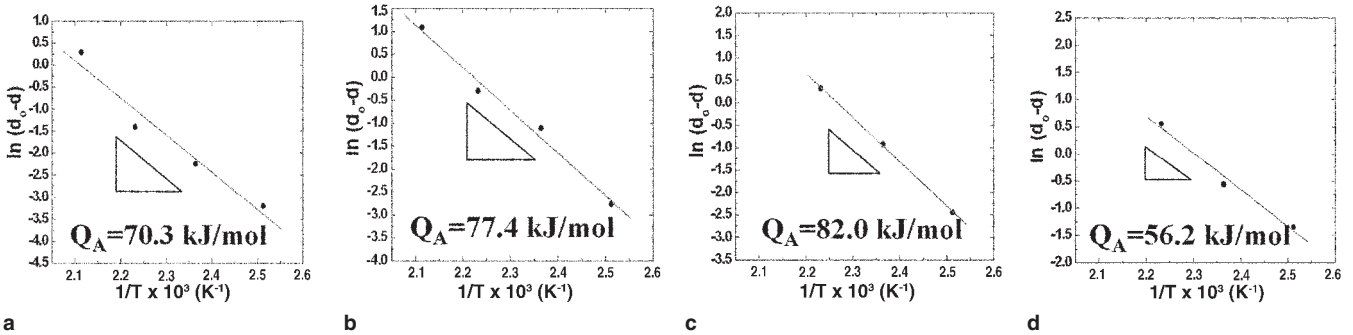


a b c d

Fig. 18. The Arrhenius plots of ln $(d - d_0)$ versus 1/T at various aging times: (a) 125 h, (b) 300 h, (c) 500 h, and (d) 1,000 h.

5at.%Au. The Au atoms in the quaternary IMC originated from an immersion Au-plated layer on the electroless Ni-P UBM. At higher temperature aging, the $(Ni,Cu)_3Sn_4$ IMC formed underneath the quaternary IMC. In contrast to reflowing, all IMCs formed during aging were well attached on the electroless Ni UBM. Higher activation energy in aging than in reflowing implies that diffusion of Cu, Ni, and Sn in solid solder would be more difficult than that in liquid solder.

## ACKNOWLEDGEMENTS

This work was supported by the Center for Electronic Packaging Materials of Korea Science and Engineering Foundation.

## REFERENCES

1. J.W. Jang, D.R. Frear, T.Y. Lee, and K.N. Tu, *J. Appl. Phys.* 88, 6359 (2000).
2. S.K. Kang et al., *Proc. 51st Electron. Comp. and Technology Conf.* (Piscataway, NJ: IEEE, 2001), pp. 448–454.
3. K. Zeng, V. Vuorinen, and J.K. Kivilahti, *Proc. 51st Electron. Comp. Technology Conf.* (Piscataway, NJ: IEEE, 2001), pp. 693–698.
4. K.Y. Lee, M. Li, D.R. Olsen, and W.T. Chen, *Proc. 51st Electron. Comp. Technology Conf.* (Piscataway, NJ: IEEE, 2001), pp. 478–485.
5. A. Zribi, L. Zavalij, P. Borgesen, A. Primavera, G. Westby, and E.J. Cotts, *Proc. 51st Electron. Comp. Technology Conf.* (Piscataway, NJ: IEEE, 2001), pp. 687–692.
6. M. Schaefer, R.A. Fournelle, and J. Liang, *J. Electron. Mater.* 27, 1167 (1998).